Bioconjugate Chemistry

Article

pubs.acs.org/bc

Macrocyclic Peptides Self-Assemble into Robust Vesicles with Molecular Recognition Capabilities

Woo-jin Jeong and Yong-beom Lim*

Translational Research Center for Protein Function Control and Department of Materials Science & Engineering, Yonsei University, Seoul 120-749, Korea

Supporting Information

ABSTRACT: In this study, we developed macrocyclic peptide building blocks that formed self-assembled peptide vesicles with molecular recognition capabilities. Macrocyclic peptides were significantly different from conventional amphiphiles, in that they could self-assemble into vesicles at very high hydrophilic-to-total mass ratios. The flexibility of the hydrophobic self-assembly segment was critical for vesicle formation. The unique features of this peptide vesicle system include a homogeneous size distribution, unusually small size, and robust structural and thermal stability. The peptide vesicles successfully entrapped a hydrophilic model drug, released the payload very slowly, and were internalized by cells in a highly efficient manner. Moreover, the peptide vesicles exhibited molecular recognition capabilities, in that they selectively bound to target RNA through surface-displayed peptides. This study demonstrates that self-assembled peptide vesicles can be used as strong intracellular delivery vehicles that recognize specific biomacromolecular targets.

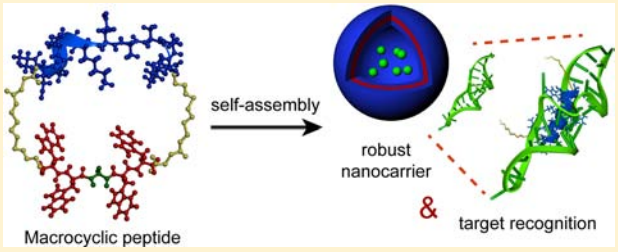

INTRODUCTION

Peptide-based molecular self-assembly is a powerful method for developing functional biomaterials. Taking advantage of the versatile and modular properties of peptides, a number of intriguing supramolecular approaches have been developed for the bottom-up fabrication of self-assembled peptide nanostructures (SPNs).[1−7] One of the main advantages of using SPNs is that the assembled nanostructures can be designed with the molecular recognition properties of peptides.[8,9] Moreover, SPNs can display multiple bioactive peptides on their surface. This multivalency has the potential to considerably reinforce binding affinity and specificity compared to monomolecular species.[10−12] Furthermore, well-organized peptide nanostructures demonstrate remarkable heat stability, which has been attributed to cooperative noncovalent interactions that occur during self-assembly.[13−15]

SPNs have been fabricated in many different types of morphologies, including one-dimensional (1D) objects (cylindrical micelles,[16] nanoribbons,[17] nanotubes,[18] and helix bundles[19]), two-dimensional (2D) objects (nanosheets[20] and nanorings/barrels[21]), and three-dimensional (3D) objects (vesicles[22]). Vesicles are spherical molecular assemblies that enclose the solvent within a bilayer of amphiphilic molecules. In biology, vesicles form the membranes of cells and many cellular organelles. Vesicles assembled from synthetic amphiphiles have been widely used to deliver entrapped molecules and drugs to cells.

Despite the numerous examples of vesicular structures formed by lipids, small molecular weight amphiphiles, and block copolymers, peptides typically assemble into 1D objects. Reports on peptide-based self-assembled vesicles are uncommon and typically have employed rather unusual approaches.[22−27] Otherwise, peptides have been shown to assemble into vesicle-like spheres or sacs.[28−30] This dearth of multidimensional peptide structures is most likely due to the fact that peptides are not well-suited for vesicular structure assembly. The planarity of the peptide bond restricts the flexibility of the polypeptide chain, the presence of hydrogen bonds impose directionality during assembly, and the chirality of amino acids imparts handedness to the overall self-assembly process. All of these effects diminish the flexibility of the polypeptide chain, thus rendering peptide aggregation into vesicular structures challenging. Therefore, it is difficult to reliably predict the self-assembly of peptides based on the simple rules of volume fraction.[23,31]

Macrocyclic peptides (MCPs), whose amino- and carboxyl-termini are linked by a covalent bond, possess unique physical,[32] chemical,[33] and biological[34] characteristics due to their conformational constraints. MCPs can also be used as building blocks for self-assembly.[8,9,22,35−37] Self-assembling MCPs typically consist of three functional segments (i.e., a self-assembling segment, hydrophilic/bioactive segment, and linker segment; Figure 1). During self-assembly, the entire hydrophilic/bioactive segment of an MCP can be exposed to the aqueous environment because the segment lies parallel to the assembled structure (Figure 1a). In contrast, only the distal

Received: August 7, 2014
Revised: August 31, 2014
Published: October 7, 2014

dx.doi.org/10.1021/bc500367z | Bioconjugate Chem. 2014, 25, 1996−2003

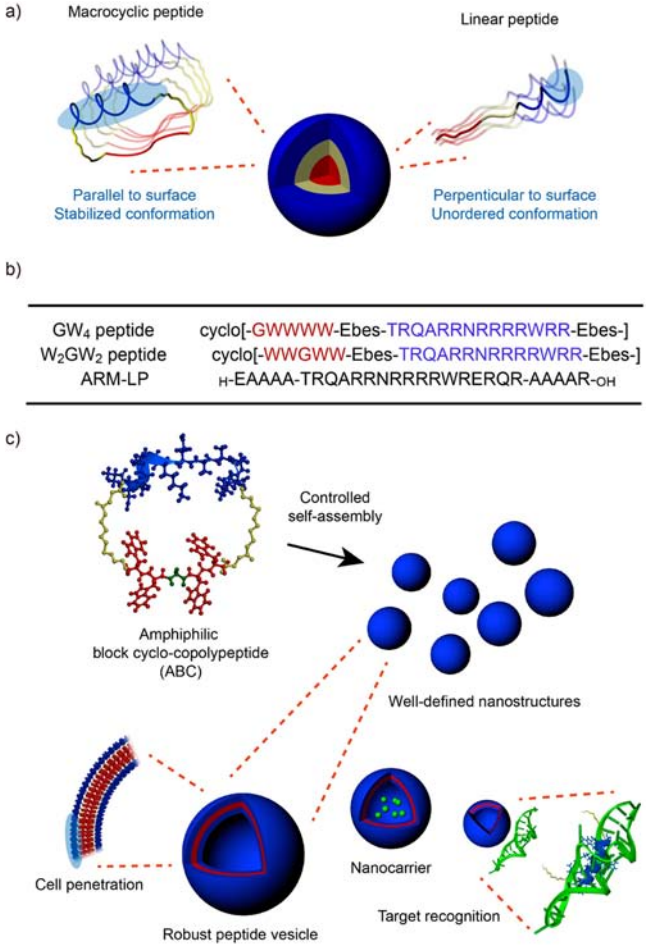

Figure 1. Self-assembly of macrocyclic peptides for robust vesicle formation with RNA molecular recognition capability. (a) Comparison of the orientations of a cyclic peptide and a linear peptide on the surface of self-assembled structures. The self-assembling segment, hydrophilic/bioactive segment, and linker segment are indicated in red, blue, and yellow, respectively. (b) Sequences of the amphiphilic block cyclo-copolypeptides (ABCs) used in this study. (c) Schematic diagram showing robust vesicle formation from the ABC peptides, and intracellular delivery of entrapped model drugs and RNA target recognition by the peptide vesicles.

end of the hydrophilic/bioactive segment of a conventional linear peptide can be exposed in a densely packed assembly, which could limit the target recognition capabilities of the bioactive segment.

In this study, we report the rational design of self-assembling MCP building blocks (amphiphilic block cyclo-copolypeptides; ABCs) for developing self-assembled peptide vesicles with molecular recognition capabilities (Figure 1). The arginine-rich motif (ARM) peptide from the human immunodeficiency virus type-1 (HIV-1) Rev protein was utilized as the hydrophilic/bioactive segment.[38,39] The aims of this study were to understand the critical factors responsible for peptide vesicle formation, to probe the self-assembly behaviors of ABC-type building blocks, and to develop a vesicular delivery system with molecular recognition functions.

RESULTS AND DISCUSSION

We designed an ABC building block that consists of a hydrophobic segment with four consecutive tryptophan residues, a hydrophilic/bioactive segment based on the Rev ARM peptide, and flexible linkers that covalently connect the two disparate segments (GW_4 peptide, Figures 1b and 2a). The

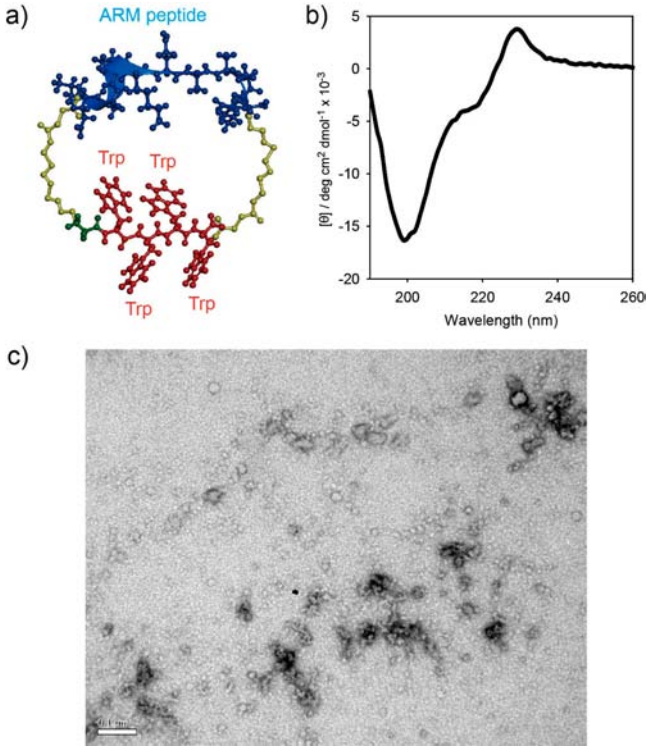

Figure 2. Characterization of the self-assembly behavior of the GW_4 ABC peptide. (a) Molecular structure. (b) CD spectrum in water at room temperature (*r.t.*) (c) TEM image (bar = 100 nm).

Rev protein interacts with the HIV-1 Rev response element (RRE) RNA in an α-helical conformation, which enables the nuclear export of intron-containing viral mRNAs encoding proteins essential for HIV-1 replication. During the viral life cycle, ARM also acts as nuclear localization signal (NLS) for the Rev protein.[40]

We first examined the self-assembly behavior of the peptides by investigating the conformation of the GW_4 peptide in self-assembled aggregates (Figure 2b). Experiments were typically performed in aqueous solution with the peptide concentration of 5−10 μM. The circular dichroism (CD) data showed a positive band at 229 nm, which indicated an interaction between aromatic chromophores (in this case, the tryptophan residues).[41] This result suggests that the tryptophan residues in the hydrophobic segment were in close proximity, due to hydrophobic and $\pi-\pi$ stacking interactions during the aggregation of the GW_4 peptides. Transmission electron microscopy (TEM) imaging of the nanostructural morphology revealed that the aggregation process was not precisely controlled, leading to the formation of various irregular aggregates (Figure 2c). We speculated that this heterogeneous aggregate formation likely arose from the lack of flexibility in the hydrophobic segment, which may have prevented tight hydrophobic packing of the peptide molecules.

To confer increased flexibility on the hydrophobic segment, we moved a glycine from the N-terminal region to the middle portion of the hydrophobic segment (Figures 1b and 3a; W_2GW_2 peptide). CD analysis confirmed the aromatic interaction at 229 nm, indicating that the W_2GW_2 peptides

dx.doi.org/10.1021/bc500367z | Bioconjugate Chem. 2014, 25, 1996−2003

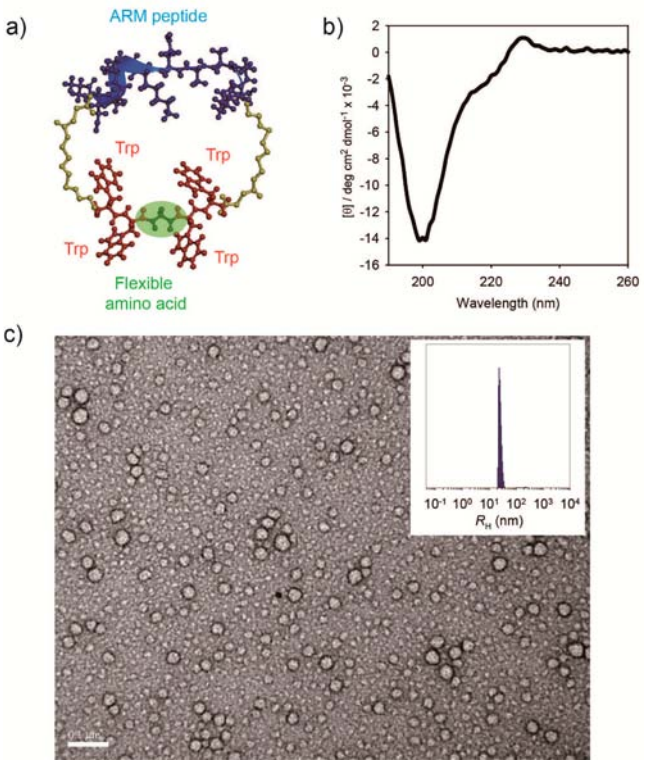

Figure 3. Characterization of the self-assembly behavior of W_2GW_2 ABC peptide. (a) Molecular structure. (b) CD spectrum in water at *r.t.* (c) TEM image (bar = 100 nm). Inset: DLS analysis of self-assembled nanostructures.

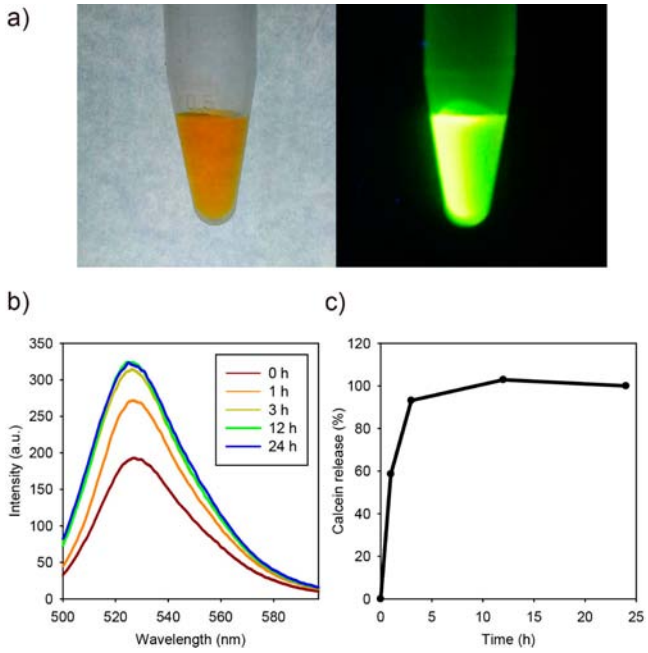

Figure 4. Entrapment and release of calcein from the W_2GW_2 peptide vesicles. (a) Early elution fraction in phosphate buffered saline (PBS) from gel filtration chromatography. Images taken under ambient light (left) and UV illumination (right). (b) Fluorescence spectra following treatment of the vesicles with Triton X-100 (2%, v/v). (c) Time-dependent calcein release profile.

assembled in a manner similar to the GW_4 peptides (i.e., hydrophobic and $\pi-\pi$ interactions). However, the repositioning of the single glycine residue significantly influenced the nanostructural morphology and homogeneity of the W_2GW_2 peptides (Figure 3c). TEM imaging showed the formation of regularly shaped spherical objects that were 27 ± 5 nm in diameter (Supporting Information Figure S3). The dynamic light scattering (DLS) analysis indicated that the average hydrodynamic radius (R_H) of the nanostructures was ~23 nm. The difference in the average size calculated by TEM and DLS likely occurred because the hydrophilic chain was hydrated by the solutions used for DLS analysis, whereas the sample was dry for TEM imaging.[42] The results suggest that inserting the pliable amino acid glycine increased the overall flexibility of the hydrophobic chain, which, in combination with the reduced mobility of the macrocyclic peptide, reinforced the internal hydrophobic packing of the molecular assembly.[43] The spherical nanostructures we observed were more likely to be vesicles than micelles, as the size of the nanostructures was much greater than twice the maximum molecular length of the cyclic peptides.[22]

To verify the identity of the vesicular nanostructures, we next performed an encapsulation experiment using a water-soluble fluorescent molecule, calcein.[26] To assemble the vesicles, the W_2GW_2 peptide and calcein were mixed together in a buffer solution and sonicated. Large assemblies were separated from smaller molecular weight species (including free calcein molecules) by gel filtration chromatography. The early elution fraction that contained the peptide nanostructures exhibited bright green calcein fluorescence, indicating successful encapsulation of the dye within the vesicular nanostructures (Figure 4a).

We further confirmed the vesicular properties of the W_2GW_2 peptide assembly by conducting a leakage assay. We observed an increase in fluorescence intensity when the vesicles were disrupted using Triton X-100, indicating the dequenching of calcein fluorescence by the release of the dye from the confined environment (Figure 4b). The time-dependent fluorescence measurements indicate that the entrapped calcein was released gradually (Figure 4c). These data further support the vesicular nanostructure of the W_2GW_2 peptide assembly. Interestingly, the release kinetics was very slow and plateaued at approximately 12 h. For most vesicular nanostructures, the complete release of encapsulated molecules typically occurs within several minutes.[44−50] The prolonged release kinetics that we observed in this study suggests that the vesicles formed by W_2GW_2 peptide self-assembly exhibit very high structural robustness.

Amphiphilic polymers generally require a hydrophilic-to-total mass ratio ($f_{hydrophilic}$) of approximately 35% for vesicular assembly, while molecules with $f_{hydrophilic}$ > 45% are more likely to assemble into micellar structures.[51] However, the $f_{hydrophilic}$ for the W_2GW_2 peptide is approximately 75%. Self-assembly into vesicular structures is unusual at this very high $f_{hydrophilic}$ value. This interesting result is likely due to the constrained characteristics of the cyclic molecule, efficient packing of the hydrophobic segments, and strong association between the aromatic residues.

To further investigate the robustness of the W_2GW_2 peptide vesicles, we analyzed the thermal stability of the structures using CD spectroscopy. The results suggested that the vesicular assemblies maintained their conformational integrity even at

dx.doi.org/10.1021/bc500367z | *Bioconjugate Chem.* 2014, 25, 1996−2003

highly elevated temperatures, up to 85 °C (Figure 5a and b). This high thermal stability is likely due to the formation of a

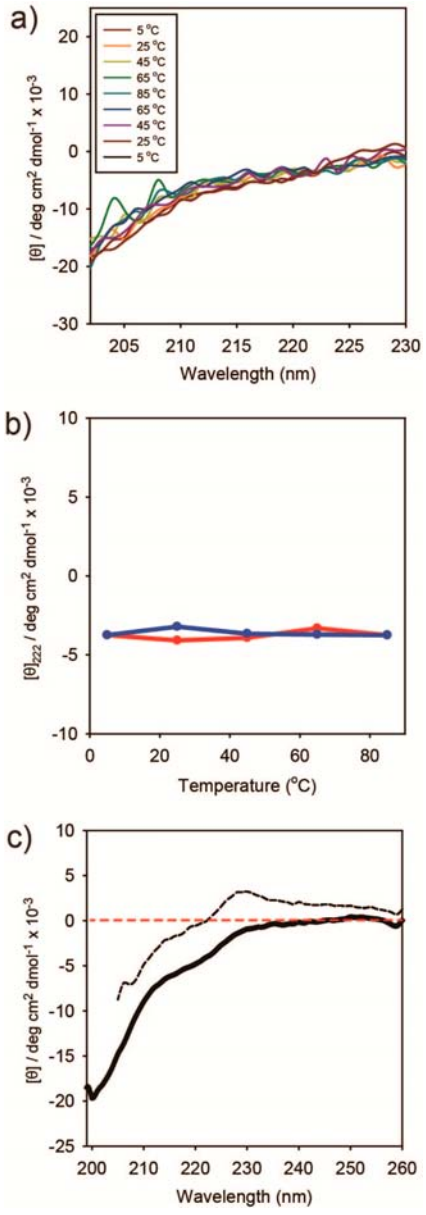

Figure 5. Thermal stability of the W_2GW_2 peptide vesicles. (a) Temperature-dependent CD spectra in PBS. (b) Changes in the molecular ellipticity at 222 nm (α-helix). Forward scan (red) and backward scan (blue) of the temperature ramp experiment. (c) CD spectra of the peptide in pure water (solid line) and in 8 M urea (dashed line).

strongly hydrophobic core and cooperative self-assembly.[15,52] As a negative control, we incubated the peptide in 8 M urea, which is strongly denaturing. The significant decrease in molecular ellipticity at 222 nm (α-helix) indicated the denaturation and/or disassembly of the vesicles (Figure 5c). This supports the hypothesis that self-assembly induces α-helix stabilization[8,9,35] and correlates well with the thermal stability data. Overall, the leakage assay and temperature-dependent conformational analysis demonstrate the structural and thermal robustness of the W_2GW_2 peptide vesicles.

Next, we assessed the ability of the peptide vesicles to transport model drugs into cells. Rev facilitates cell penetration and nuclear localization, enabling the cytoplasmic and even intranuclear delivery of conjugated entities.[53] We hypothesized that the peptide vesicle system would exhibit similar delivery capabilities. To test this, we treated HeLa cells with W_2GW_2 peptide vesicles containing calcein and monitored the delivery and intracellular localization of the calcein marker. After 4 h of treatment at 37 °C, every cell exhibited bright calcein fluorescence, indicating efficient intracellular delivery (Figure 6 and Supporting Information Figure S4). The green

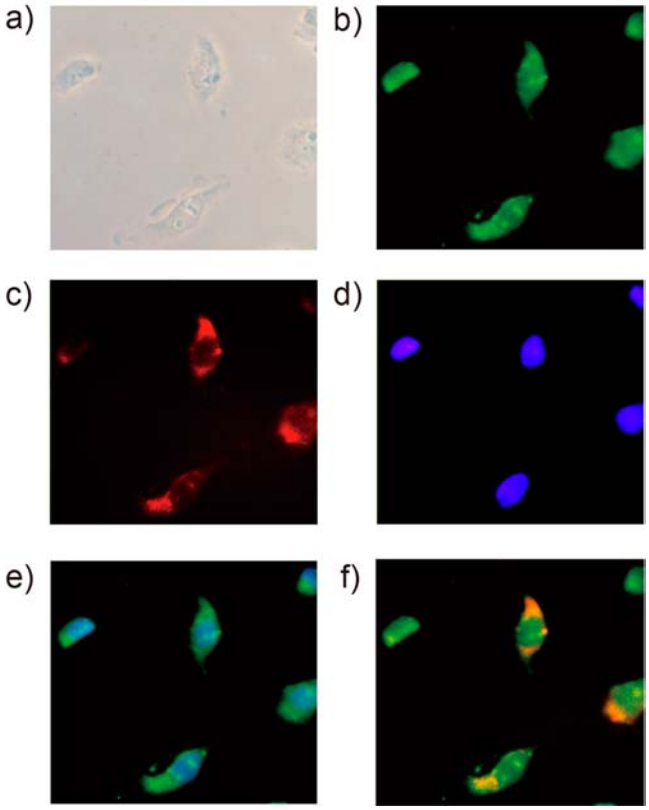

Figure 6. Intracellular delivery of the W_2GW_2 peptide vesicles and encapsulated calcein to HeLa cells. (a) Bright-field image. (b) Green (calcein) fluorescence. (c) Red fluorescence from LysoTracker Red DND-99. (d) Counterstaining of the nuclei with DAPI. (e) Merged image of calcein and DAPI fluorescence. (f) Merged image of calcein and LysoTracker fluorescence.

fluorescence of calcein was widely distributed throughout the entire cell including nucleus as well as cytosol. The LysoTracker stains the endosomes and lysosomes. Dual color imaging of calcein fluorescence and red LysoTracker fluorescence (yellow) indicated that the vesicles could enter the cell via endocytosis (Figure 6f).

Because the W_2GW_2 peptide vesicles are decorated with the bioactive Rev ARM peptide, we next evaluated whether the vesicles can recognize a specific target. The Rev ARM peptide has a high propensity for helicity and binds its target RRE RNA in an α-helical conformation. The degree of α-helix preorganization significantly affects binding affinity and specificity.[54] Thus, we investigated the conformational status of the Rev ARM peptide within the nanostructure by CD spectroscopy. As is shown in Figure 3b, the W_2GW_2 peptide within the vesicular nanostructures rarely formed a helical

dx.doi.org/10.1021/bc500367z | Bioconjugate Chem. 2014, 25, 1996−2003

structure in pure water. However, the CD spectrum of the W_2GW_2 peptide in PBS exhibited a broad negative band at approximately 222 nm, a signature of α-helices, which has offset the positive band at 229 nm (Figure 7a). To clarify this solvent-dependent conformational change, we synthesized a peptide that contained only the Rev ARM segment (ARM-LP peptide) and subjected it to CD analysis under various solvent conditions (Figure 7c). In pure water, the ARM-LP peptide exhibited minimal helicity. In contrast, the ARM-LP peptide dissolved in PBS exhibited somewhat enhanced α-helicity, as indicated by the increase in 222 nm signal. Subtraction of the two spectra indicated the presence of typical α-helix bands with dual minima at 208 and 222 nm, indicating that helicity increased in the buffered saline solvent (Figure 7d).[55] Similarly, the solvent-dependent difference spectrum for the W_2GW_2 peptide vesicle indicated that the α-helical conformation was stabilized in PBS condition (Figure 7b). This increased helicity of the Rev ARM peptide in buffered saline is likely due in part to the decreased repulsion between the charged arginine residues and the inhibition of nonspecific charge interactions.

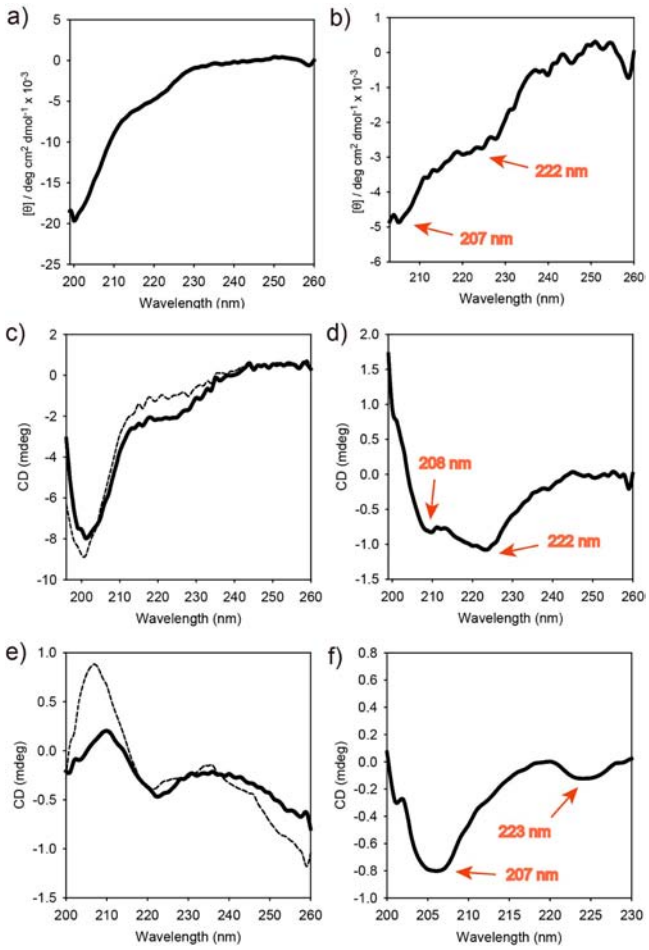

Figure 7. Molecular recognition capabilities of the peptide vesicles. (a) CD spectrum of the W_2GW_2 peptide vesicle in PBS. (b) Difference spectrum of the W_2GW_2 peptide vesicle (CD spectrum in water was subtracted from that in PBS, i.e., PBS minus water). (c) CD spectra of the ARM-LP peptide in water (dashed line) and in PBS (solid line). (d) Difference spectrum of the ARM-LP peptide (PBS minus water). (e) CD spectra of the W_2GW_2 peptide vesicle and RRE RNA complexes in PBS (peptide to RNA molar ratio: 5 to 1). Solid line: wild-type RNA; dashed line: mutant RNA. (f) Difference spectrum for the various RRE sequences (the wild-type minus the mutant).

We next investigated the RNA recognition properties of the W_2GW_2 peptide vesicle by CD spectroscopy. We utilized two types of RRE RNA: wild-type RRE RNA, which exhibits high affinity and specificity for the Rev ARM peptide, and a mutant RRE RNA (a G46-C74 to C46-G74 mutation), which exhibits impaired binding to the Rev ARM peptide (Supporting Information Figure S5). After 1 h of vesicle-RNA complex formation at room temperature, the wild-type and mutant complexes were analyzed by CD spectroscopy (Figure 7e). The difference spectra from the spectroscopic data (the wild-type complex minus the mutant complex) revealed that the degree of helix stabilization for the Rev ARM peptide segment of the W_2GW_2 peptide vesicle was higher for the wild-type complex than for the mutant complex, as shown by the dual negative minima at 207 and 223 nm (Figure 7f). These results demonstrate the specificity of the peptide for wild-type RRE RNA. Therefore, the W_2GW_2 peptide vesicles exhibit RRE RNA molecular recognition capabilities.

■ CONCLUSIONS

We have developed functional peptide vesicles using macrocyclic peptides. The flexibility of the hydrophobic self-assembly segment was critical for the successful aggregation of ABC-type building blocks into vesicle nanostructures. The size distribution of the ABC peptide vesicles was fairly homogeneous. The vesicles were unusually small, and were structurally and thermally robust. The peptide vesicles successfully entrapped a hydrophilic fluorescent probe (model drug), released the payload very slowly, and were internalized very efficiently by cells due to the cell-penetrating and nucleus localization activities of the Rev ARM peptide. Importantly, the peptide vesicles exhibit molecular recognition capabilities, as they were able to selectively bind to the target RNA of Rev protein. This study demonstrates that the self-assembly of ABC-type cyclic peptides is significantly different from that of conventional amphiphiles. The ABCs self-assemble into vesicles at very high $f_{\text{hydrophilic}}$ and form unusually small vesicles considering the peptides' molecular weight (3000−4000 Da). These peptide vesicles also exhibit unique molecular recognition properties. We expect that peptide vesicles with molecular recognition function can be developed as controlled release drug delivery carriers that can simultaneously modulate biomacromolecular interactions (e.g., protein−RNA, protein−DNA, and protein−protein interactions).

■ MATERIALS AND METHODS

Materials. Fmoc-amino acids and coupling reagents were purchased from Novabiochem (Germany) and Anaspec (USA). General chemicals were obtained from Sigma-Aldrich (USA) and Merck (Germany). The oligoethylene glycol-based linker, *N*-(Fmoc-8-amino-3,6-dioxaoctyl)succinamic acid (Fmoc-PEG2-Suc-OH or Fmoc-Ebes-OH), was purchased from Anaspec. The HPLC solvents were purchased from Fisher Scientific (USA). The tissue culture reagents were obtained from Invitrogen (USA).

Peptide Synthesis. The 2-chlorotrityl resin was first preloaded with Fmoc-Ebes-OH. Further amino acid couplings was performed on a Tribute peptide synthesizer on a 0.1 mmol scale (Protein Technologies). Standard amino acid protecting groups were used for the synthesis. For the head-to-tail

dx.doi.org/10.1021/bc500367z | *Bioconjugate Chem.* 2014, 25, 1996−2003

cyclization reaction, the N-terminal Fmoc-group was deprotected following the completion of the final amino acid coupling. The protected peptide fragment (20 μmol) was liberated from the resin by using a cleavage cocktail of acetic acid/2,2,2-trifluoroethanol (TFE)/methylene chloride (MC) (2:2:6). After an appropriate amount of time (~1 to 2 h), the resin was removed by filtration and the filtrate was recovered (4 mL × 2). Finally, the resin was washed three times with the cleavage cocktail for complete recovery. Hexane was added to the filtrate to remove acetic acid as an azeotrope with hexane. The protected peptide fragment was obtained as a white powder following repeated evaporation cycles (the dissolution of the peptide fragment in MC, hexane addition, and evaporation).

The peptides were cyclized by head-to-tail cyclization between the N-terminal amine and C-terminal carboxylic acid groups. For cyclization, typically 10 μmol of the protected peptide fragment and 40 μmol of DIPEA were dissolved in DMF (10 mL) and transferred into a syringe. Then, 10 μmol of HATU was dissolved in DMF (10 mL) and transferred into another syringe. To achieve pseudo-high-dilution conditions, the two solutions were added together to a stirred solution of 1 μmol HATU and 10 μmol HOBt in DMF (10 mL) at a rate of 0.05 mL/min by using a syringe pump. Once the addition was complete, the reaction mixture was further stirred for ~5 h. Following DMF evaporation, the residue was dissolved in MC, and then *tert*-butyl methyl ether/hexane was added to triturate the cyclized and protected peptide fragment (three times). The peptide fragment was treated with a cleavage cocktail (TFA/TIS/water; 95:2.5 2.5) for 3 h and then was then triturated with *tert*-butyl methyl ether. The peptides were purified by reverse-phase HPLC (water−acetonitrile with 0.1% TFA). The molecular weight was confirmed by MALDI-TOF mass spectrometry. The purity of the peptides was >95%, as determined by analytical HPLC. The peptide concentration was determined spectrophotometrically in water/acetonitrile (1:1) using the molar extinction coefficient of tryptophan (5502 M^{-1} cm^{-1}) at 280 nm.

CD Spectroscopy (CD). The CD spectra were recorded using a Chirascan Circular Dichroism spectrometer equipped with a Peltier temperature controller (Applied Photophysics., Ltd.). The CD spectra of samples were recorded from 260 to 190 nm using a 2 mm path-length cuvette. The molar ellipticity was calculated per amino acid residue.

Transmission Electron Microscopy (TEM). One microliter of sample was placed onto a carbon-coated copper grid and dried completely. Then, 1 μL of water was added for 1 min to eliminate salt crystals and was then quickly wicked off using filter paper. Next, 2 μL of a 2% (w/v) uranyl acetate solution was added for 1 min, and the excess solution was wicked off using filter paper. The specimen was observed with a JEOL-JEM 2010 instrument operating at 120 kV. The data were analyzed with DigitalMicrograph software.

Dynamic Light Scattering (DLS). DLS experiments were performed at room temperature using an ALV/CGS-3 compact goniometer system equipped with a He−Ne laser operating at 632.8 nm. The detector optics employed optical fibers coupled to an ALV/SO-SIPD/DUAL detection unit, which employed an EMI PM-28B power supply and an ALV/PM-PD preamplifier/discriminator. The signal analyzer was an ALV-5000/E/WIN multiple-τ digital correlator with 288 exponentially spaced channels. The scattering angle was 90°. The size distribution was determined using a constrained-regularization method.

Leakage Experiment. The W_2GW_2 peptide vesicles containing calcein were treated with 2% (v/v) Triton X-100 with gentle shaking at room temperature. Samples were removed periodically, and their steady-state fluorescence spectra were recorded using a PerkinElmer LS-55 fluorescence spectrophotometer in 1 cm path length quartz cuvettes. To measure the calcein fluorescence, the samples were excited at 495 nm. Excitation and emission slits with a nominal bandpass of 5 nm were used for measurement. For the analysis of the time-course release data, the percentage of released calcein at different time points was calculated according to the following formula

$$\%\text{release} = 100(I_t - I_0)/(I_\infty - I_0)$$

where I_t is the fluorescence intensity at a specific time point, I_0 is the fluorescence intensity without detergent treatment, and I_∞ is the fluorescence intensity at complete vesicle disruption.

Tissue-Culture and Intracellular-Delivery Experiments. For microscopic observation of the intracellular delivery of the calcein-containing vesicular nanostructures, HeLa cells (1×10^4) were seeded in an 8-well Lab-tek II chambered cover-glass system (Nunc) in Dulbecco's modified Eagle's medium (DMEM) with 10% fetal bovine serum (FBS) and cultured overnight at 37 °C. The cells were washed with Dulbecco's phosphate-buffered saline (DPBS) and treated with the vesicular structures for 4 h. Then, the sample solution was removed and the cells were further incubated with 50 nM of LysoTracker Red DND-99 (Invitrogen) and 1.5 μM of 4′,6-diamidino-2-phenylindole (DAPI, Sigma-Aldrich) for 1 h. The cells were visualized using a fluorescence microscope (IX 71, Olympus, Japan).

■ ASSOCIATED CONTENT

Ⓢ Supporting Information

Chemical structures, MALDI-TOF MS spectra, size distribution data, cellular localization data, and RNA structures. This material is available free of charge via the Internet at http://pubs.acs.org.

■ AUTHOR INFORMATION

Corresponding Author

*E-mail: yblim@yonsei.ac.kr.

Notes

The authors declare no competing financial interest.

■ ACKNOWLEDGMENTS

This work was supported by grants from the National Research Foundation (NRF) of Korea (2012R1A1A2006453 and 2009-0083522).

■ REFERENCES

(1) Lim, Y. B., Moon, K. S., and Lee, M. (2009) Recent advances in functional supramolecular nanostructures assembled from bioactive building blocks. *Chem. Soc. Rev. 38*, 925−934.

(2) Charbonneau, C., Kleijn, J. M., and Cohen Stuart, M. A. (2014) Subtle charge balance controls surface-nucleated self-assembly of designed biopolymers. *ACS Nano 8*, 2328−2335.

(3) Micklitsch, C. M., Knerr, P. J., Branco, M. C., Nagarkar, R., Pochan, D. J., and Schneider, J. P. (2011) Zinc-triggered hydrogelation of a self-assembling beta-hairpin peptide. *Angew. Chem., Int. Ed. 50*, 1577−1579.

(4) Yolamanova, M., Meier, C., Shaytan, A. K., Vas, V., Bertoncini, C. W., Arnold, F., Zirafi, O., Usmani, S. M., Muller, J. A., Sauter, D., Goffinet, C., Palesch, D., Walther, P., Roan, N. R., Geiger, H., Lunov, O., Simmet, T., Bohne, J., Schrezenmeier, H., Schwarz, K., Standker, L., Forssmann, W. G., Salvatella, X., Khalatur, P. G., Khokhlov, A. R., Knowles, T. P., Weil, T., Kirchhoff, F., and Munch, J. (2013) Peptide nanofibrils boost retroviral gene transfer and provide a rapid means for concentrating viruses. *Nat. Nanotechnol. 8*, 130−136.
(5) Li, D., Furukawa, H., Deng, H., Liu, C., Yaghi, O. M., and Eisenberg, D. S. (2014) Designed amyloid fibers as materials for selective carbon dioxide capture. *Proc. Natl. Acad. Sci. U.S.A. 111*, 191−196.
(6) Debnath, S., Roy, S., and Ulijn, R. V. (2013) Peptide nanofibers with dynamic instability through nonequilibrium biocatalytic assembly. *J. Am. Chem. Soc. 135*, 16789−16792.
(7) Altunbas, A., Lee, S. J., Rajasekaran, S. A., Schneider, J. P., and Pochan, D. J. (2011) Encapsulation of curcumin in self-assembling peptide hydrogels as injectable drug delivery vehicles. *Biomaterials 32*, 5906−5914.
(8) Jeong, W. J., Choi, S. J., Choi, J. S., and Lim, Y. B. (2013) Chameleon-like self-assembling peptides for adaptable biorecognition nanohybrids. *ACS Nano 7*, 6850−6857.
(9) Jeong, W. J., Lee, M. S., and Lim, Y. B. (2013) Helix stabilized, thermostable, and protease-resistant self-assembled peptide nanostructures as potential inhibitors of protein-protein interactions. *Biomacromolecules 14*, 2684−2689.
(10) Fasting, C., Schalley, C. A., Weber, M., Seitz, O., Hecht, S., Koksch, B., Dernedde, J., Graf, C., Knapp, E. W., and Haag, R. (2012) Multivalency as a chemical organization and action principle. *Angew. Chem., Int. Ed. 51*, 10472−10498.
(11) Mammen, M., Choi, S. K., and Whitesides, G. M. (1998) Polyvalent interactions in biological systems: Implications for design and use of multivalent ligands and inhibitors. *Angew. Chem., Int. Ed. 37*, 2755−2794.
(12) Lim, Y. B., and Lee, M. (2007) Self-assembled multivalent carbohydrate ligands. *Org. Biomol. Chem. 5*, 401−405.
(13) Hartgerink, J. D., Granja, J. R., Milligan, R. A., and Ghadiri, M. R. (1996) Self-assembling peptide nanotubes. *J. Am. Chem. Soc. 118*, 43−50.
(14) Lesk, A. M. (2003) Hydrophobicity - getting into hot water. *Biophys. Chem. 105*, 179−182.
(15) Han, S. H., Lee, M. K., and Lim, Y. B. (2013) Bioinspired self-assembled peptide nanofibers with thermostable multivalent alpha-helices. *Biomacromolecules 14*, 1594−1599.
(16) Tovar, J. D., Claussen, R. C., and Stupp, S. I. (2005) Probing the interior of peptide amphiphile supramolecular aggregates. *J. Am. Chem. Soc. 127*, 7337−7345.
(17) Han, S., Kim, D., Han, S. H., Kim, N. H., Kim, S. H., and Lim, Y. B. (2012) Structural and conformational dynamics of self-assembling bioactive beta-sheet peptide nanostructures decorated with multivalent RNA-binding peptides. *J. Am. Chem. Soc. 134*, 16047−16053.
(18) Reches, M., and Gazit, E. (2003) Casting metal nanowires within discrete self-assembled peptide nanotubes. *Science 300*, 625−627.
(19) Fletcher, J. M., Harniman, R. L., Barnes, F. R., Boyle, A. L., Collins, A., Mantell, J., Sharp, T. H., Antognozzi, M., Booth, P. J., Linden, N., Miles, M. J., Sessions, R. B., Verkade, P., and Woolfson, D. N. (2013) Self-assembling cages from coiled-coil peptide modules. *Science 340*, 595−599.
(20) Moon, K. S., Lee, E., Lim, Y. B., and Lee, M. (2008) Bioactive molecular sheets from self-assembly of polymerizable peptides. *Chem. Commun.*, 4001−4003.
(21) Park, I. S., Yoon, Y. R., Jung, M., Kim, K., Park, S., Shin, S., Lim, Y. B., and Lee, M. (2011) Designer nanorings with functional cavities from self-assembling beta-sheet peptides. *Chem.—Asian J. 6*, 452−458.
(22) Choi, S. J., Jeong, W. J., Kang, S. K., Lee, M., Kim, E., Ryu, D. Y., and Lim, Y. B. (2012) Differential self-assembly behaviors of cyclic and linear peptides. *Biomacromolecules 13*, 1991−1995.
(23) Bellomo, E. G., Wyrsta, M. D., Pakstis, L., Pochan, D. J., and Deming, T. J. (2004) Stimuli-responsive polypeptide vesicles by conformation-specific assembly. *Nat. Mater. 3*, 244−248.
(24) Chung, E. K., Lee, E., Lim, Y. B., and Lee, M. (2010) Cyclic peptide facial amphiphile preprogrammed to self-assemble into bioactive peptide capsules. *Chem.—Eur. J. 16*, 5305−5309.
(25) Matsuura, K., Murasato, K., and Kimizuka, N. (2005) Artificial peptide-nanospheres self-assembled from three-way junctions of beta-sheet-forming peptides. *J. Am. Chem. Soc. 127*, 10148−10149.
(26) van Hell, A. J., Costa, C. I. C. A., Flesch, F. M., Sutter, M., Jiskoot, W., Crommelin, D. J. A., Hennink, W. E., and Mastrobattista, E. (2007) Self-assembly of recombinant amphiphilic oligopeptides into vesicles. *Biomacromolecules 8*, 2753−2761.
(27) Yoon, Y. R., Lim, Y. B., Lee, E., and Lee, M. (2008) Self-assembly of a peptide rod-coil: a polyproline rod and a cell-penetrating peptide Tat coil. *Chem. Commun.*, 1892−1894.
(28) Reches, M., and Gazit, E. (2004) Formation of closed-cage nanostructures by self-assembly of aromatic dipeptides. *Nano Lett. 4*, 581−585.
(29) Maity, S., Nir, S., and Reches, M. (2014) Co-assembly of aromatic dipeptides into spherical structures that are similar in morphology to red and white blood cells. *J. Mater. Chem. B 2*, 2583−2591.
(30) Carvajal, D., Bitton, R., Mantei, J. R., Velichko, Y. S., Stupp, S. I., and Shull, K. R. (2010) Physical properties of hierarchically ordered self-assembled planar and spherical membranes. *Soft Matter 6*, 1816−1823.
(31) Israelachvili, J. N. (1985) *Intermolecular and surface forces: with applications to colloidal and biological systems*, pp xv, 296, Academic Press, London.
(32) Yamagata, K., Goto, Y., Nishimasu, H., Morimoto, J., Ishitani, R., Dohmae, N., Takeda, N., Nagai, R., Komuro, I., Suga, H., and Nureki, O. (2014) Structural basis for potent inhibition of SIRT2 deacetylase by a macrocyclic peptide inducing dynamic structural change. *Structure 22*, 345−352.
(33) Sun, Y. X., and Kollman, P. A. (1995) Quantitation and nature of the macrocyclic effect - K+ complexation with 18-crown-6 and pentaglyme. *J. Am. Chem. Soc. 117*, 3599−3604.
(34) Huai, Q., Kim, H. Y., Liu, Y. D., Zhao, Y. D., Mondragon, A., Liu, J. O., and Ke, H. M. (2002) Crystal structure of calcineurin-cyclophilin-cyclosporin shows common but distinct recognition of immunophilin-drug complexes. *Proc. Natl. Acad. Sci. U.S.A. 99*, 12037−12042.
(35) Lim, Y. B., Moon, K. S., and Lee, M. (2009) Stabilization of an alpha helix by beta-sheet-mediated self-assembly of a macrocyclic peptide. *Angew. Chem., Int. Ed. 48*, 1601−1605.
(36) Ghadiri, M. R., Granja, J. R., Milligan, R. A., Mcree, D. E., and Khazanovich, N. (1993) Self-assembling organic nanotubes based on a cyclic peptide architecture. *Nature 366*, 324−327.
(37) Kim, B., Choi, S. J., Han, S. H., Choi, K. Y., and Lim, Y. B. (2013) Stabilization of alpha-helices by the self-assembly of macrocyclic peptides on the surface of gold nanoparticles for molecular recognition. *Chem. Commun. 49*, 7617−7619.
(38) Pollard, V. W., and Malim, M. H. (1998) The HIV-1 Rev protein. *Annu. Rev. Microbiol. 52*, 491−532.
(39) Fang, X., Wang, J., O'Carroll, I. P., Mitchell, M., Zuo, X., Wang, Y., Yu, P., Liu, Y., Rausch, J. W., Dyba, M. A., Kjems, J., Schwieters, C. D., Seifert, S., Winans, R. E., Watts, N. R., Stahl, S. J., Wingfield, P. T., Byrd, R. A., Le Grice, S. F., Rein, A., and Wang, Y. X. (2013) An unusual topological structure of the HIV-1 Rev response element. *Cell 155*, 594−605.
(40) Groom, H. C., Anderson, E. C., and Lever, A. M. (2009) Rev: beyond nuclear export. *J. Gen. Virol. 90*, 1303−1318.
(41) Cochran, A. G., Skelton, N. J., and Starovasnik, M. A. (2001) Tryptophan zippers: Stable, monomeric beta-hairpins. *Proc. Natl. Acad. Sci. U.S.A. 98*, 5578−5583.
(42) Lim, Y. B., Lee, E., and Lee, M. (2007) Controlled bioactive nanostructures from self-assembly of peptide building blocks. *Angew. Chem., Int. Ed. 46*, 9011−9014.

(43) Zhu, B. Y., Zhou, N. E., Kay, C. M., and Hodges, R. S. (1993) Packing and hydrophobicity effects on protein folding and stability - effects of beta-branched amino-acids, valine and isoleucine, on the formation and stability of 2-stranded alpha-helical coiled coils leucine zippers. *Protein Sci. 2*, 383−394.
(44) Benachir, T., and Lafleur, M. (1995) Study of vesicle leakage induced by melittin. *Biochim. Biophys. Acta, Biomembr. 1235*, 452−460.
(45) Boudreault, P. L., and Voyer, N. (2007) Synthesis, characterization and cytolytic activity of alpha-helical amphiphilic peptide nanostructures containing crown ethers. *Org. Biomol. Chem. 5*, 1459−1465.
(46) Coleman, A. C., Beierle, J. M., Stuart, M. C., Macia, B., Caroli, G., Mika, J. T., van Dijken, D. J., Chen, J., Browne, W. R., and Feringa, B. L. (2011) Light-induced disassembly of self-assembled vesicle-capped nanotubes observed in real time. *Nat. Nanotechnol. 6*, 547−552.
(47) De Maria, P., Fontana, A., Gasbarri, C., and Velluto, D. (2006) Effects of fullerene guests on the stability of 1-palmitoyl-2-oleoylphosphatidylcholine liposomes. *Soft Matter 2*, 595−602.
(48) Holme, M. N., Fedotenko, I. A., Abegg, D., Althaus, J., Babel, L., Favarger, F., Reiter, R., Tanasescu, R., Zaffalon, P. L., Ziegler, A., Muller, B., Saxer, T., and Zumbuehl, A. (2012) Shear-stress sensitive lenticular vesicles for targeted drug delivery. *Nat. Nanotechnol. 7*, 536−543.
(49) Vandenburg, Y. R., Smith, B. D., Biron, E., and Voyer, N. (2002) Membrane disruption ability of facially amphiphilic helical peptides. *Chem. Commun.*, 1694−1695.
(50) Yasayan, G., Redhead, M., Magnusson, J. P., Spain, S. G., Allen, S., Davies, M., Alexander, C., and Fernandez-Trillo, F. (2012) Well-defined polymeric vesicles with high stability and modulation of cell uptake by a simple coating protocol. *Polym. Chem. 3*, 2596−2604.
(51) Discher, D. E., and Eisenberg, A. (2002) Polymer vesicles. *Science 297*, 967−973.
(52) Forns, P., Lauer-Fields, J. L., Gao, S., and Fields, G. B. (2000) Induction of protein-like molecular architecture by monoalkyl hydrocarbon chains. *Biopolymers 54*, 531−546.
(53) Bolhassani, A. (2011) Potential efficacy of cell-penetrating peptides for nucleic acid and drug delivery in cancer. *Biochim. Biophys. Acta, Rev. Cancer 1816*, 232−246.
(54) Tan, R. Y., Chen, L., Buettner, J. A., Hudson, D., and Frankel, A. D. (1993) RNA recognition by an isolated alpha-helix. *Cell 73*, 1031−1040.
(55) Han, S., and Lim, Y. B. (2014) Covalent capture of alpha-helical peptides in polymer hydrogel network for polyacrylamide gel stabilization electrophoresis. *J. Polym. Sci., Part A: Polym. Chem. 52*, 596−599.